Biophysical Journal, Volume *113*

Supplemental Information

Homodimeric Kinesin-2 KIF3CC Promotes Microtubule Dynamics

Stephanie Guzik-Lendrum, Ivan Rayment, and Susan P. Gilbert

SUPPORTING MATERIALS AND METHODS

Homodimeric and Heterodimeric KIF3 Motor Constructs

The *Mus musculus* KIF3A, KIF3B and KIF3C plasmids that were used herein for expression of the KIF3CC, KIF3AC, and KIF3AB motors, as well as the truncation of KIF3C that generated KIF3CCΔL11, were described in detail previously (1, 2). Briefly, to generate stable dimers of KIF3CC, KIF3AC and KIF3CCΔL11, a segment of the dimerization motif from EB1 was fused as an in-register extension of the native coiled-coil to the C-terminus of the construct. Previous work has established that the C-terminal addition of this segment of EB1 sequence to the KIF3AC motor did not enhance MT binding nor did it alter run length of KIF3AC (2). The polypeptide for KIF3CC contained the native N-terminal motor domain sequence, native neck linker, and native α7 helix, with a C-terminally fused EB1 sequence that matched the coiled-coil registry of the helix (*bold*), TEV protease site (*italicized*) with linker residues (*plain font*), and a His_8-tag (*underlined*).
KIF3C: KIF3C(Met^{1}-Leu^{396})-
DFYFGKLRNIELICQENEGENDPVLQRIVDILYATDETTS*ENLYFQ*GASHHHHHHHH (predicted M.W. = 49,759)

KIF3AC was the product of co-expressing the KIF3C plasmid detailed above with a similarly-designed KIF3A plasmid that replaced the His_8-tag with a StrepII affinity purification tag (*underlined*):
KIF3A-EB1: KIF3A(Met^{1}-Leu^{374})-
DFYFGKLRNIELICQENEGENDPVLQRIVDILYATDETTS*ENLYFQ*GASNWSHPQFEK
(predicted M.W. = 48,559)

For KIF3CCΔL11, the plasmid for the native KIF3C with the EB1 fusion was modified to delete the KIF3C-specific extension of Loop L11 (Asn^{259}-Ser^{284}), as well as to incorporate a KIF3C-specific substitution at Pro^{258} with Ala (predicted M.W. = 47,689) as previously described (2).

For KIF3AB, the stable heterodimer was generated through the use of a synthetic heterodimerization domain (SHD) motif instead of EB1. The SHD created strong heterodimeric associations through a pairwise affiliation between an acidic motif and a basic motif on either construct that established heterodimeric KIF3AB complexes during expression, minimized the probability of homodimerization, and stabilized the native coiled-coils of the heterodimeric motors (1). In these constructs, KIF3A contained an acidic fusion helix (AHD, *bold*) and KIF3B contained a basic fusion helix (BHD, *bold*) followed by a TEV protease site (*italicized*) and linker residues (*plain font*), with C-terminally fused StrepII and His_8-affinity tags on KIF3A and KIF3B, respectively (*both underlined*).
KIF3A-AHD: KIF3A(Met^{1}-Glu^{376})-**LEKEIAALEKEIAALEK**TTS*ENLYFQ*GASNWSHPQFEK (predicted M.W. = 46,341)
KIF3B-BHD: KIF3B(Met^{1}-Lys^{371})-**LKEKIAALKEKIAALKE**TTS*ENLYFQ*GASHHHHHHHH
(predicted M.W. = 45,790)

Protein Expression and Purification

All KIF3 motors were bacterially expressed as previously reported (2) in *E. coli* BL21-CodonPlus (DE3)-RIL cells (Stratagene, La Jolla, CA). Homodimers were expressed in bacteria transformed with single plasmids followed by selection on lysogeny broth (LB) plates containing

100 μg/mL ampicillin and 10 μg/mL chloramphenicol. Heterodimers resulted from co-transformation of two plasmids into bacteria that were then grown on LB selection plates containing 100 μg/mL ampicillin, 50 μg/mL kanamycin, and 10 μg/mL chloramphenicol. Positive colonies were selected and grown in LB culture at 37°C to A_{600} of ~0.5. Cultures were then chilled in an ice bath to 16°C for 20 min before expression was induced with the addition of 0.1 mM isopropyl β-D-1-thiogalactopyranoside (IPTG). Cultures were maintained at 16°C with shaking at 185 rpm for ~16-18 h. Cells were then collected by centrifugation (Sorvall Evolution Centrifuge; Sorvall SLC-6000 rotor, 4400 *x g* at 4°C for 30 min) and resuspended with gentle stirring at 4°C for 60 min in lysis buffer (10 mM sodium phosphate buffer, pH 7.2, 300 mM NaCl, 2 mM $MgCl_2$, 0.1 mM EGTA, 10 mM PMSF, 1 mM DTT, 0.2 mM ATP and 30 mM imidazole at a ratio of 1 g cells to 3 mL lysis buffer. Resuspended cell pellets were then frozen in liquid N_2 and stored at -80°C prior to purification. Upon thawing, the frozen cell suspension was adjusted to a ratio of 1 g cells to 10 mL lysis buffer plus 0.1 mg/mL lysozyme, incubated in an ice bath with stirring for 30 min followed by lysis through a series of three freeze/thaw cycles that alternate between liquid N_2 and a 37°C water bath. The cell lysate was clarified by ultracentrifugation (Beckman Coulter Optima TLX Ultracentrifuge; Beckman Ti45 rotor at 125,000 x *g*) and the supernatant loaded onto a HisTrap FF Ni^{2+}-NTA column (GE Lifesciences, Piscataway, NJ) that had been pre-equilibrated with Ni^{2+} Binding Buffer (20 mM sodium phosphate buffer, pH 7.2, 300 mM NaCl, 2 mM $MgCl_2$, 0.1 mM EGTA, 1 mM DTT, 0.2 mM ATP, and 30 mM imidazole). The loaded column continued to wash with Ni^{2+} Binding Buffer until the absorbance reached baseline. The protein was then eluted with a linear gradient (Ni^{2+} Binding Buffer at 30 mM imidazole to 300 mM imidazole, pH 7.2).

For homodimeric motors (KIF3CC and KIF3CCΔL11) with His_8 tagged protein, positive fractions from the Ni^{2+}-NTA column were pooled and concentrated, and were further purified by gel filtration on an HPLC gel filtration column (Superose™ 10/300, GE Lifesciences, Piscataway, NJ) on a Beckman Coulter System Gold HPLC (Fullerton, CA). Elution was detected by intrinsic fluorescence (Jasco FP-2020, Victoria, British Columbia) in 20 mM HEPES, pH 7.2 with KOH, 0.1 mM EDTA, 0.1 mM EGTA, 5 mM magnesium acetate, 50 mM potassium acetate, 1 mM DTT plus 200 mM NaCl.

For heterodimeric motors (KIF3AC and KIF3AB), the Ni^{2+}-NTA column selected for any complex that included a copy of KIF3B or KIF3C. To isolate purified heterodimers, the pool of His_8-tagged proteins was subjected to purification for the StrepII tag on KIF3A to ensure both proteins were present in each purified heterodimeric complex. First, positive fractions from the Ni^{2+}-NTA column were pooled and transferred to a StrepIITactin™ column (GE Lifesciences) that had been pre-equilibrated with StrepII Column Buffer (20 mM sodium phosphate buffer, pH 7.2, 300 mM NaCl, 2 mM $MgCl_2$, 0.1 mM EGTA, 1 mM DTT, 0.2 mM ATP). The loaded column was washed with StrepII Column Buffer until the absorbance reached baseline, followed by elution of the heterodimeric motors (StrepII Column Buffer with 2.5 mM desthiobiotin). Fractions were run on an SDS-PAGE gel and only the fractions with a 1:1 ratio of the KIF3 polypeptides were pooled, concentrated, and dialyzed overnight at 4°C against 20 mM HEPES, pH 7.2 with KOH, 0.1 mM EGTA, 5 mM magnesium acetate, 50 mM potassium acetate, 1 mM DTT, 5% sucrose, and 100 mM NaCl.

Qdot Spiking for Single Molecule Localization

Imaging single motors within the dynamic MT assay requires single molecule concentrations of motor. However, working with such low motor concentrations also resulted in a large number of

MTs that behaved as though no KIF3CC motor was bound. Thus, we adapted a previously published technique (6) that maintains the saturating concentration of KIF3CC used for our initial experiments (50 nM KIF3CC) while also visualizing single motors. In this method, termed spiking, the pool of KIF3CC motors in the microscopy chamber with dynamic MTs were spiked with a small subpopulation of KIF3CC that had been labeled with Qdots.

For the spiking experiments, Qdots (525-Streptavidin conjugate, Life Technologies, Carlsbad, CA) were first mixed at a 4:1 ratio with biotinylated Penta-His antibody (Qiagen, Valencia, CA) in PME80. This initial mixture combined 7.8 μL of Qdots (1.0 mM stock) with 1.5 μL of antibody (1.3 mM stock) and 2.7 μL 5x PME80 (400 mM PIPES, pH 6.9, 25 mM $MgCl_2$, and 5 mM EGTA). This resulted in concentrations of 650 nM Qdots and 162.5 nM antibody, which were then incubated for 60 min at room temperature to generate Qdot•antibody complexes.

In a separate tube, KIF3 motors were prepared by an initial dilution to 500 nM in ATPase buffer (20 mM HEPES, pH 7.2 with KOH, 0.1 mM EDTA, 0.1 mM EGTA, 5 mM magnesium acetate, 50 mM potassium acetate, 1 mM DTT, 5% sucrose). After the incubation of Qdot•antibody complex was complete, 6.2 μL of the Qdot•antibody complex was combined with 2 μL of 500 nM KIF3CC, which resulted in a Labeled Stock intermediate that diluted the Qdot•antibody complexes to 126 nM and incorporated 122 nM KIF3CC. This Labeled Stock was incubated for 60 min on ice to allow enough time for the motors to occupy all potential binding sites. Ultimately, the Labeled Stock generated the pool of motors that became the subpopulation of KIF3CC visualized by the single molecule assay.

Once the Labeled Stock incubation was complete, it was used to “spike” unlabeled KIF3CC. For this process, a separate dilution of motor was made at 6.1 μM KIF3CC of which 1.8 μL was supplemented with the full volume (8.2 μL) of Labeled Stock. This reaction mix generated 10 μL of Working Stock solution, that contained both the visible subpopulation of 100 nM KIF3CC (bound to Qdot•antibody complex, itself at 103 nM in the Working Stock) and an additional 1.1 μM unlabeled KIF3CC, thus, generating a total combined concentration of 1.2 μM KIF3CC (labeled and unlabeled combined) in the Working Stock. This Working Stock was then added to the MT Extension Mix used for stimulating MT dynamics (1.3 μL of Working Stock at 1.2 μM KIF3CC into a final volume of 31 μL Extension Mix). Each preparation of Extension Mix generated three microscopy chambers (10 μL of Extension Mix into each chamber) with the final motor concentration at 50 nM KIF3CC, spiked with 4 nM Qdot•antibody•KIF3CC that can be visualized at 488 nm in each microscopy chamber. This method was also used for the other KIF3 motors localized with the spiking assay.

Note that this method differs significantly from our traditional Qdot assay, which relies on a 1:10 ratio of motors to Qdots to ensure single motor binding to each Qdot (2). Instead, the method reported here starts with excess Qdots incubated with a limiting concentration of antibody. This creates a condition in which only a subpopulation of Qdots is competent to bind His_8-tagged motors. The concentration of motor to be labeled was thus determined based on the concentration of available Qdot•antibody complexes to saturate the competent Qdot•antibody complex.

SUPPORTING DATA ANALYSIS

Quantification of KIF3CC at the MT plus end

Percentage of KIF3CC visible by TIRF microscopy:
[KIF3CC]: 50 nM KIF3CC dimer in microscopy chamber, which includes 4 nM Qdot•KIF3CC
4 nM Qdot•KIF3CC per 50 nM KIF3CC total = 8% of population visible.
Therefore, 92% of the KIF3CC population is not detectable.

Two calculations for KIF3CC load on MTs:

*Note that Qdots and Qdot-motor complexes bind to the non-silanized surface of the perfusion chamber. Therefore, both methods provide a lower limit to the estimate of motors present per MT.

1) *As determined by the average number of Qdots per MT extension*

Analysis was conducted from data collected over 3 days of replicate experiments, using 2 Fields of View (FOV) from each day = total 6 FOVs
Counts were taken from the first extension off of each MT seed

Compiled data from each FOV:
Total number of Qdot•KIF3CC = 911
Total number of initial MT extensions = 682
911 Qdot•KIF3CC per 682 MTs = 1.3 Qdot•KIF3CC per MT

Extrapolated for total population of KIF3CC:
Labeling ratio: 92% unlabeled KIF3CC / 8% Qdot•KIF3CC
= 11.5 unlabeled KIF3CC per 1 Qdot•KIF3CC

1.3 Qdot•KIF3CC per MT x 11.5 labeling ratio
= 14.95 unlabeled KIF3CC + 1.3 Qdot•KIF3CC

= **16.25 KIF3CC motors per MT**

2) *As determined by average counts of Qdots and MTs per FOV*

Analysis was conducted from data collected over 3 days of replicate experiments, using 3 Fields of View (FOV) from each day = total 9 FOVs
Counts were taken from the first extension off of each MT seed

Averages from compiled data:
Average number of Qdot•KIF3CC per FOV = 152
Average number of initial MT extensions per FOV = 114

Extrapolated for total population of KIF3CC:
Labeling ratio: 92% unlabeled KIF3CC / 8% Qdot•KIF3CC
= 11.5 unlabeled KIF3CC per 1 Qdot•KIF3CC

152 Qdot•KIF3CC per FOV x 11.5
= 1748 unlabeled KIF3CC + 152 Qdot•KIF3CC
= 1900 KIF3CC motors per FOV / 114 MTs

= **16.7 KIF3CC motors per MT**

Figure S1, related to Figure 1. Heterodimeric KIF3AC Does Not promote MT Catastrophe.

A

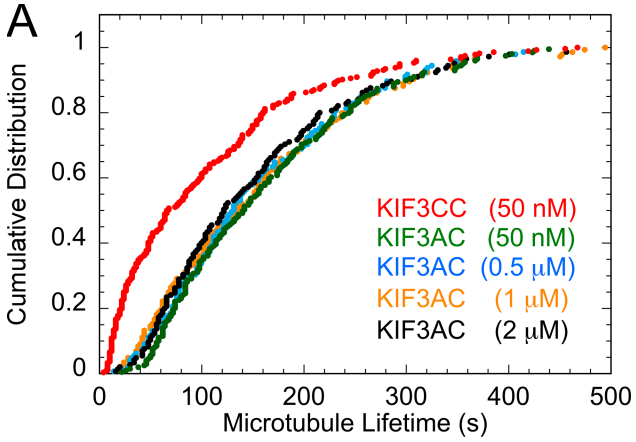

B

	N	Step Parameter	Catastrophe Frequency (min^{-1})
KIF3CC (50 nM)	252	1.00 ± 0.08	0.47 ± 0.038
KIF3AC			
50 nM	177	2.70 ± 0.27	0.24 ± 0.011
0.5 μM	145	2.65 ± 0.27	0.24 ± 0.013
1 μM	144	2.61 ± 0.23	0.24 ± 0.013
2 μM	145	2.64 ± 0.26	0.24 ± 0.011

(***A***) Cumulative Distribution plot as a function of MT lifetime in the presence of varying concentrations of KIF3AC ($K_{1/2,MT}$ = 133 nM) in comparison to 50 nM KIF3CC ($K_{1/2,MT}$ = 44 nM), each at 2 mM MgATP (2). See also Fig. 1*D* for additional Cumulative Distribution plot comparisons to the KIF3CC dataset. (***B***) The gamma fit (Eq. 1) applied to each MT lifetime data set (Probability Density Function plot) provided the step parameters for the titration of KIF3AC in the dynamic MT assay. The population catastrophe frequency values were calculated as the number of catastrophe events that occur per minute in the presence of each motor concentration. All values reported as ± SEM, and N values correlate to those in panel *A*.

Figure S2, related to Figure 5. KIF3CC Binds the MT Lattice but Resides for Short Periods of Time at the MT Plus-Tip.

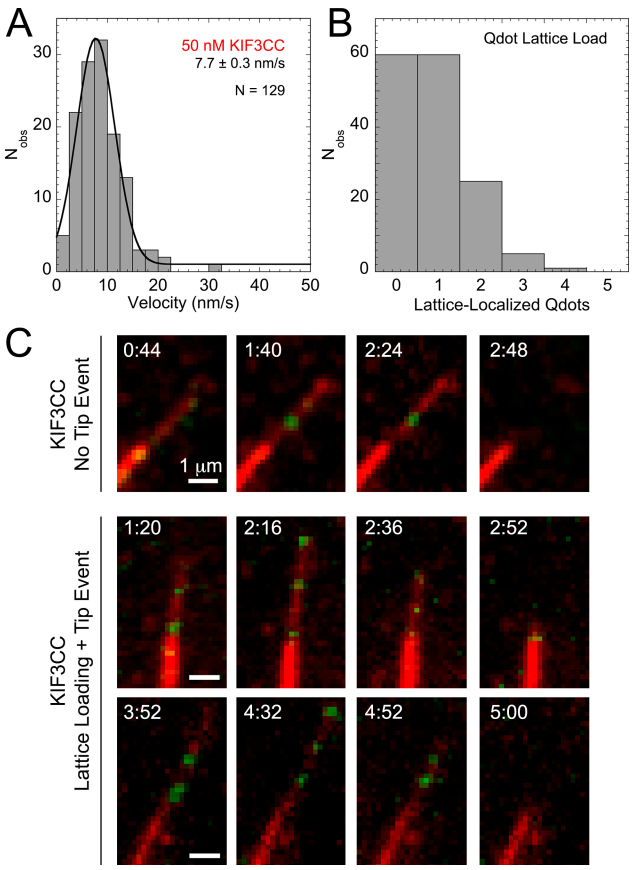

(***A***) Histogram of the velocity of lattice-bound KIF3CC motors moving processively during MT extension events. A Gaussian fit to the data provides the average velocity at 7.7 ± 0.3 nm/s, reported as ± SEM. See also Fig. 5*B*. (***B***) Histogram of the number of Qdot•KIF3CC complexes bound along the lattice of dynamic MT extensions. Lattice-bound Qdots were defined separately from tip-associated events or those associated with the GMPCPP-stabilized seed. The height of each histogram bin represents the number of MT extensions that were observed to have from 0 to 5 lattice-bound Qdots immediately prior to catastrophe. Out of a total of 151 MT extensions that occurred from 34 seeds over 10 min, there were 60 MT extensions with no lattice-bound Qdots (bin 0) prior to catastrophe and 91 MT extensions with lattice-bound Qdots. Combined, a total of 129 lattice-bound Qdots were observed. Each visible Qdot•KIF3CC represents ~8% of the population of KIF3CC motors in these experiments. Thus, the presence of lattice-bound Qdots implies considerable KIF3CC coverage along the MT lattice and that this lattice-bound population of KIF3CC does not inhibit MT extension nor does it promote catastrophe. (***C***) Representative dual-channel images of KIF3CC (*green*) bound along the dynamic MT lattice (*red; brightly labeled GMPCPP seeds with dimly labeled MT extensions*). Four time points are provided for each example. In the absence of a visible tip localization event (*top row*), the first two time points correspond to the growing MT extension prior to a Qdot landing on the MT and the frame during which the Qdot lands and begins moving processively along the MT lattice. In examples with a visible MT tip localization event (*bottom 2 rows*), the first two time points correspond to a frame with KIF3CC-Qdots processively stepping along the MT followed by the frame during which the Qdot landed on the MT plus-end. For all examples shown, the third and fourth time points correspond to: the frame immediately after the initiation of MT catastrophe, and the endpoint of catastrophe at the GMPCPP seed. The timestamps on each image are relative to the beginning of the raw data image acquisition (0:00). Scale bars, 1 μm.

Table S1, related to Figure 2. Compiled Step Parameters for KIF3CC and Controls.

	Step Parameter	N
No Motor	2.62 ± 0.23	230
KIF3CC (50 nM)	1.00 ± 0.08	252
No Nucleotide	2.67 ± 0.26	194
2 mM MgAMPPNP	2.60 ± 0.23	229
KIF3AB (50 nM)	2.62 ± 0.25	201
KIF3AC (50 nM)	2.70 ± 0.27	177
KIF3CCΔL11 (50 nM)	2.72 ± 0.26	186

Compiled step parameter values representing the number of MT aging steps accumulated for each condition prior to catastrophe. These values were determined from the gamma fit of the PDF plots of raw MT lifetime data. All values are reported as ± SEM from the fit.

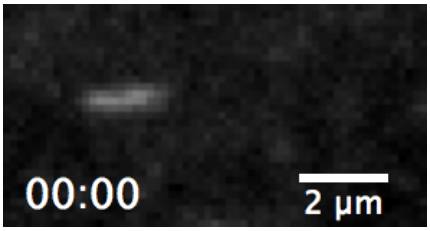

Movie S1. MT dynamics in the absence of KIF3CC in conditions with 10 μM tubulin (1:8.5 labeling ratio), 1 mM MgGTP and 2 mM MgATP. Average rate of elongation 16.8 ± 0.3 nm/s with an average length of 2.5 ± 0.1 μm. Video playback speed at 120x real-time.

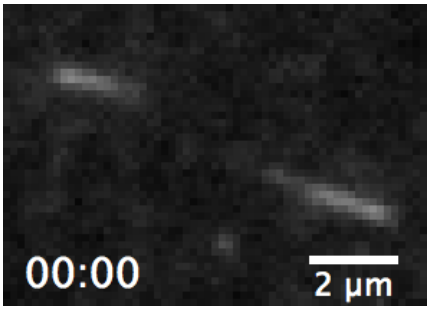

Movie S2. MT dynamics are altered by the presence of 50 nM KIF3CC dimer, with extension conditions including 10 μM tubulin (1:8.5 labeling ratio), 1 mM MgGTP and 2 mM MgATP. The average rate of elongation is 24.5 ± 0.8 nm/s and average length 1.5 ± 0.1 μm. Video playback speed at 120x real-time. Two MTs are shown.

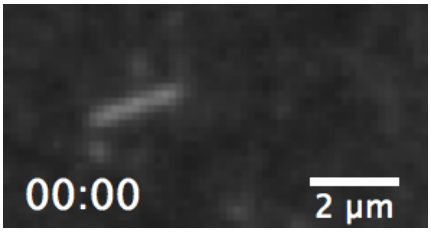

Movie S3. MT dynamics are unaffected by the presence of 50 nM KIF3AC. Extension conditions include 10 μM tubulin (1:8.5 labeling ratio), 1 mM MgGTP and 2 mM MgATP. Average elongation rate 18.1 ± 0.5 nm/s, average length 2.3 ± 0.1 μm. Video playback speed at 120x real-time.

Movie S4. MT dynamics are unaffected by the presence of 50 nM KIF3CCΔL11 in which the extended loop L11 of both KIF3C motors has been truncated to the length seen throughout the rest of the kinesin superfamily. Extension conditions include 10 μM tubulin (1:8.5 labeling ratio), 1 mM MgGTP and 2 mM MgATP. Average elongation rate 19.5 ± 0.5 nm/s, average length 2.8 ± 0.1 μm. Video playback speed at 120x real-time.

SUPPORTING REFERENCES

1. Albracht, C. D., K. C. Rank, S. Obrzut, I. Rayment, and S. P. Gilbert. 2014. Kinesin-2 KIF3AB Exhibits Novel ATPase Characteristics. J Biol Chem 289:27836-27848.
2. Guzik-Lendrum, S., K. C. Rank, B. M. Bensel, K. C. Taylor, I. Rayment, and S. P. Gilbert. 2015. Kinesin-2 KIF3AC and KIF3AB Can Drive Long-Range Transport along Microtubules. Biophys J 109:1472-1482.
3. Coombes, C. E., A. Yamamoto, M. R. Kenzie, D. J. Odde, and M. K. Gardner. 2013. Evolving tip structures can explain age-dependent microtubule catastrophe. Curr Biol 23:1342-1348.
4. Demchouk, A. O., M. K. Gardner, and D. J. Odde. 2011. Microtubule Tip Tracking and Tip Structures at the Nanometer Scale Using Digital Fluorescence Microscopy. Cell Mol Bioeng 4:192-204.
5. Prahl, L. S., B. T. Castle, M. K. Gardner, and D. J. Odde. 2014. Quantitative analysis of microtubule self-assembly kinetics and tip structure. Methods Enzymol 540:35-52.
6. Varga, V., C. Leduc, V. Bormuth, S. Diez, and J. Howard. 2009. Kinesin-8 motors act cooperatively to mediate length-dependent microtubule depolymerization. Cell 138:1174-1183.